# Recommendations on setup in simulating atmospheric gravity waves under conventionally neutral boundary layer conditions

Khan, M.A.; Watson, S.J.; Allaerts, D.J.N.; Churchfield, Matthew

**DOI**
10.1088/1742-6596/2767/9/092042

**Publication date**
2025

**Document Version**
Final published version

**Published in**
Journal of Physics: Conference Series

**PAPER** • **OPEN ACCESS**

# Recommendations on setup in simulating atmospheric gravity waves under conventionally neutral boundary layer conditions

To cite this article: Mehtab A Khan *et al* 2024 *J. Phys.: Conf. Ser.* **2767** 092042

Journal of Physics: Conference Series **2767** (2024) 092042 doi:10.1088/1742-6596/2767/9/092042

# Recommendations on setup in simulating atmospheric gravity waves under conventionally neutral boundary layer conditions

**Mehtab A Khan[1], Simon J Watson[1], Dries J N Allaerts[1], and Matthew Churchfield[2]**

[1]Delft Technical University, Delft, NL
[2]National Renewable Energy Laboratory, CO, US

E-mail: m.a.khan-2@tudelft.nl

**Abstract.** Wind farm-induced atmospheric gravity waves have been the subject of recent research as they can impact wind farm performance. Pressure variations associated with gravity waves can contribute to the global blockage effect and wind farm wake recovery. Therefore, accurate numerical simulation of flow fields, where wind-farm-induced gravity waves may be produced, is important. Three main considerations in such simulations are the overall domain size, the use of Rayleigh damping near domain boundaries to dampen gravity waves, and advection damping at the inlet to prevent spurious oscillations. Often these considerations are treated ad hoc rather than systematically. This work aims to test and extend the systematic modelling of internal gravity waves proposed in a preliminary investigation to modelling of both internal and trapped gravity waves. The preliminary study identifies the length scales to set the domain and damping layer sizes and the time scale to configure the Rayleigh damping coefficient but under linearly stratified conditions. Large eddy simulations of flow through a wind farm canopy are performed under conventionally neutral boundary layer (CNBL) conditions to test the validity of proposed setups for CNBL conditions. Background atmospheric parameters, such as Froude number ($Fr$), inversion height ($H_i$), and inversion layer Froude number ($Fr_i$) control most of the atmospheric gravity wave characteristics. We validated for CBNL conditions that the effective wavelengths of the internal gravity waves are the correct length scale to configure the domain size and damping layer thickness. Likewise, the optimum damping coefficient to dampen the internal gravity waves relates to the free atmosphere's buoyancy frequency or buoyant perturbations' time scale. We infer that the damping coefficient in the inversion layer may relate to the inversion buoyancy frequency to effectively dampen the trapped gravity waves. Moreover, the advection damping length is linked to the horizontal wavelength of the trapped gravity waves in the inversion layer to prevent spurious waves at the inlet by retaining wave energy accumulation.

## 1. Introduction

Large wind farms can displace significant flow aloft, displacing low-lying inversion layers, mostly under stable surface conditions. The inversion layer displacement is the disturbance, and the distinct but stable potential temperature profiles in both the inversion layer and free atmosphere are the sources of the restoring buoyancy force required to trigger wind farm-induced atmospheric gravity waves (AGWs). Thus, AGWs include the trapped gravity waves (TGWs) inside the inversion layer that are sensitive to the inversion buoyancy frequency ($N_i$) and propagating or

evanescent internal gravity waves (IGWs) in the free atmosphere aloft that are sensitive to the Brunt-Väisälä frequency ($N$) [1, 2]. The surface stability (neutral, stable, or unstable) affects temperature profiles in the atmospheric boundary layer (ABL) and is relevant to the AGW phenomena only insofar as it affects the inversion layer height. Otherwise, AGWs exist in the inversion layer and free atmosphere, which are always stable. Gravity waves may be triggered under stable surface conditions in the ABL, but turbulence might dominate them completely.

AGWs establish pressure feedback at the wind farm scale that slows the flow upstream and might accelerate it at the downstream end of the array [3, 4]. Some researchers relate the contribution of these waves, either partially or solely, to the global blockage effect. For instance, Allaerts and Meyers argue that wind farm efficiency is reduced by up to 6% due to blockage caused by AGWs [8]. Likewise, Lanzilao and Meyers concluded from a large eddy simulation (LES) parametric study that the overall beneficial or detrimental effects of AGWs on wind farm efficiency depend on the potential temperature profile. For a single wind farm layout, they investigated 40 conventionally neutral boundary layer (CNBL) profiles, characterized by a constant potential temperature in the ABL, a jump across the inversion layer, and a stable distribution in the free atmosphere aloft. For certain CNBLs, the non-local wind farm efficiency that accounts for the blockage due to AGWs is reported as low as 26% compared to 98% for the reference neutral case with no AGWs [9]. So far, AGWs have mainly been explored with LES under CNBL conditions. The AGW dynamics for varying wind farm layouts, varying inversion heights due to changing surface stability, and other aspects critical to wind farm performance are foreseeable avenues to investigate with LES. Therefore, a thorough understanding and accurate modeling of AGWs are vital in simulating wind farms to understand the full impact of AGWs on wind farm performance.

Numerical modelling is the most viable option for studying the impact of wind-farm-induced atmospheric gravity waves on array performance. Simulating the aerodynamics of wind farms, including AGWs, must include a finite domain. This is in contrast to the Earth's atmosphere, which is horizontally periodic and vertically goes to space. Confining the simulation domain misrepresents the AGW physics at the boundaries that lead to spurious waves and reflections. For example, for the inflow/outflow boundary conditions which are used in this study, the wave energy accumulates at the inlet, especially for subcritical conditions. The reflections and accumulated wave energy at the inlet can contaminate the solution, compromising its accuracy.

Approaches used to minimize reflections are generally ad-hoc, making them difficult to implement systematically. For instance, the commonly used Rayleigh damping layers (RDLs) require rigorous tuning to determine the optimal damping coefficient and thickness for the given flow conditions [1]. Applying radiation conditions (RCs) is computationally inexpensive and effective for boundaries that perfectly match wave propagation, i.e. the wave transport speed is known [10]. However, RCs are less effective for practical flow conditions in wind farm applications as AGWs propagate inclined to the horizontal. Moreover, the flow interaction with the wind farm triggers a wave spectrum instead of a single wave. Therefore, estimating the wave transport speed is complicated, particularly in finite volume codes [11]. Lanzilao & Meyers [3] compared the performance of RDLs with RCs for wind farm LES with SPWind, a pseudo-spectral code, and found that RDLs outperformed RCs for wind farm flow situations.

The spurious waves triggered by energy accumulation at the inlet can be excluded from wind farm simulations using periodic boundary conditions instead of inflow/outflow. However, mimicking inflow/outflow while using periodic boundary conditions is done with fringes layers. A fringe layer is an RDL that can prescribe transient reference velocities and eliminate recycling the wind farm wake [3]. The fringe layer mismatches the flow conditions inside the physical domain as it attempts to maintain the precursor or user-defined reference inflow velocity, thus becoming a source of spurious waves. These fringe-trigger waves are contained in the fringe layer by advection damping introduced by Lanzilao & Meyers [3]. In principle, in the advection damping

layer, the horizontal advection of vertical velocity is eliminated by multiplying the convective term in the vertical momentum equation with a damping function, which is as follows.

$$d(x) = 1 - [F(\frac{x - x_s^d}{\delta_s^d}) - F(\frac{x - x_e^d}{\delta_e^d} + 1)] \tag{1}$$

where parameters with subscripts 's' and 'e' relate to function start and end. Thus, $x_s^d$ and $x_e^d$ are the starting and ending locations of the function. $\delta_s^d$ is the distance overlapping the fringe where the damping function gradually goes from maximum to zero while the fringe layer strength goes to zero from maximum. Likewise, $\delta_e^d$ is the region at the end where the damping function smoothly transits to the maximum. The damping function is zero in the buffer region between $\delta_s^d$ and $\delta_e^d$. Lanzilao & Meyers propose using at least eight grid points in the buffer zone for pseudo-spectral codes [3]. The lengths of these zones are suggested in [3] to be set as a fraction of the domain length. Thus, both suggestions appear ad-hoc. In our current work, we investigate if advection damping is useful with inflow/outflow boundary conditions in restricting the spurious waves triggered due to energy accumulation at the inlet.

Khan et al. propose a systematic approach to setting up wind farm simulations, including IGWs, by linking critical simulation parameters with flow parameters [11]. They idealized conditions like the free atmosphere to connect IGW wavelengths, and the Brunt-Väisälä with domain and damping layer size and RDL coefficient, respectively. This study extends Khan et al.'s [11] approach, referred to as the preliminary study here onwards, to CBNL conditions and investigates the systematic modeling of TGWs and IGWs. We also investigate if the length of the advection damping regions relates to the TGW's horizontal wavelength instead of the domain length.

## 2. Methodology

Based on preliminary results, dimensional analysis of the critical variables in simulating a CNBL, given in table 1, gives eight Pi groups. Froude number ($Fr = U/NL$) and Slope parameter $S_h = H/L$ are the only Pi groups affecting the IGW properties under linearly stratified conditions. Khan et al. show with the analytical and numerical solutions for flow over a 2D hill that the wavelengths and direction of internal waves in the free atmosphere depend on the Froude number $Fr$ [11]. $Fr$ is the ratio of flow inertia to buoyancy force for flow over the hill or wind farm of a certain length. The flow interaction with a hill or wind farm triggers several waves, which superimpose to create an effective wave with effective horizontal ($\lambda_{hor}$) and vertical ($\lambda_{ver}$) wavelength. The amplitude depends mainly on $S_h$, which is kept constant in this study. Inversion layer height ($\tilde{H}_i = H_i/H$), and Froude number ($Fr_i = U/\sqrt{g'H_i}$), where $g' = g\Delta\theta/\theta_o$ with $\Delta\theta$ being the temperature jump across the inversion layer, are important when the boundary and inversion layers are simulated. Besides the trapped wave properties, $Fr_i$ and $\tilde{H}_i$ affect inversion displacement, influencing internal wave properties in the free atmosphere. The remaining groups, $\tilde{X} = X/\lambda_{hor}$, $\tilde{L}_z = L_z/\lambda_{ver}$, $\tilde{L}_d = L_d/\lambda_{ver}$, $\xi = 1/\tau N$, are normalized simulation parameters that do not affect the wave properties.

LES of flow through wind farm canopies (WFCs) is carried out to test and refine the findings of the preliminary study for CNBL conditions. WFC is a surrogate of a wind farm that uniformly distributes its total thrust force over a control volume covering its spatial extent. The wind farm thrust is the product of WFC volume and the wind turbine thrust per unit volume. The wind turbine thrust per unit volume, as given below, is based on a fixed wind farm thrust coefficient ($C_{ft} = \frac{\pi C_t}{4S_xS_y}$), where $S_x$ and $S_y$ are non-dimensional lateral and streamwise turbine distances, normalized with the rotor diameter.

$$\frac{F_D}{V} = \frac{1}{2}\rho U^2 \frac{\pi C_t}{4S_xS_y}\frac{1}{H} \tag{2}$$

**Table 1.** The principal variables involved in simulating atmospheric gravity waves under conventionally neutral boundary layer conditions. The tested values of physical variables are inspired from [9] [12].

| Variable | Variable Type | Range of Tested Values |
|---|---|---|
| Velocity($U$) | Physical | $1\,\mathrm{m\,s^{-1}}$ to $50\,\mathrm{m\,s^{-1}}$ |
| Brunt-Väisälä frequency ($N$) | Physical | $0.005\,\mathrm{s^{-1}}$ to $0.02\,\mathrm{s^{-1}}$ |
| Inversion buoyancy frequency ($N_i$) | Physical | $0.05\,\mathrm{s^{-1}}$ to $0.2\,\mathrm{s^{-1}}$ |
| Inversion mid-point height ($H_i$) | Physical | 150 m to 1450 m |
| Half-length of hill or canopy length ($L$) | Physical | 1 km to 15 km |
| Hill or canopy height ($H$) | Physical | 16 m to 240 m |
| Domain length ($X$) | Simulation | 0.5 km to 200 km |
| Domain height ($L_z$) | Simulation | 0.3 km to 40 km |
| Damping thickness ($L_d$) | Simulation | 0.3 km to 45 km |
| Damping coefficient ($1/\tau$) | Simulation | $0.001\,\mathrm{s^{-1}}$ to $0.5\,\mathrm{s^{-1}}$ |

$H$ is the WFC height analogous to the rotor diameter, and $C_t$ is the turbine thrust coefficient. The preliminary study [11] details WFC implementation.

Simulation runs performed in this study are categorized into two sets as shown in Table 2. The first set includes non-turbulent simulations, testing the proposed setups in the preliminary study by including the CNBL temperature profiles corresponding to $Fr_i = [0.3, 0.41, 0.51, 0.92]$ and Coriolis force. We also investigated the advection damping layer and the anticipated dependency of its length ($L_a$) on the TGW wavelengths. The second set tests the proposed setup by including ground roughness and inflow turbulence. The reported $Fr_i$ cases are simulated by varying inversion heights; thus, integral scale eddy sizes would vary. Thus, the possibility of large eddy-induced IGWs is also highlighted.

**Table 2.** Set of simulations performed and key parameters investigated in each set.

| Set | $Fr$ | $Fr_i$ | Physical parameters investigated | Simulation parameters investigated |
|---|---|---|---|---|
| 1 | [0.1, 0.5] | [0.3, 0.41, 0.51, 0.92] | $\lambda$, $N_i$, $H_i$, $f$ | $\tilde{X}$, $\tilde{L}_z$, $\tilde{L}_d$, $\xi$, $\tilde{L}_a$ |
| 2 | [0.1] | [0.41, 0.51] | $H_i$, Eddy size | With & without I-RDL |

Flow is simulated with the finite volume LES codes Simulator for Wind Farm Applications (SOWFA)[5] and Toolbox fOr Stratified Convective Atmospheres (TOSCA) [4]. The potential temperature and incompressible Navier-Stokes equations are solved under non-hydrostatic conditions with the Boussinesq approximation for buoyancy. We use both codes but present mainly the TOSCA results here. We plan to use TOSCA runs by Stipa et al. [12] as references for our actuator disc resolved simulations. The numerical setup used in this study is shown in fig. 1(left). For the non-turbulent simulations, a uniform velocity at the inlet and a pressure outlet are used in the streamwise direction. The rectangular domain is periodic laterally and is 100 m wide for the non-turbulent cases. Moreover, free slip conditions are used at the bottom and top boundaries. CNBL potential temperature profiles, an example shown in fig. 1(right),

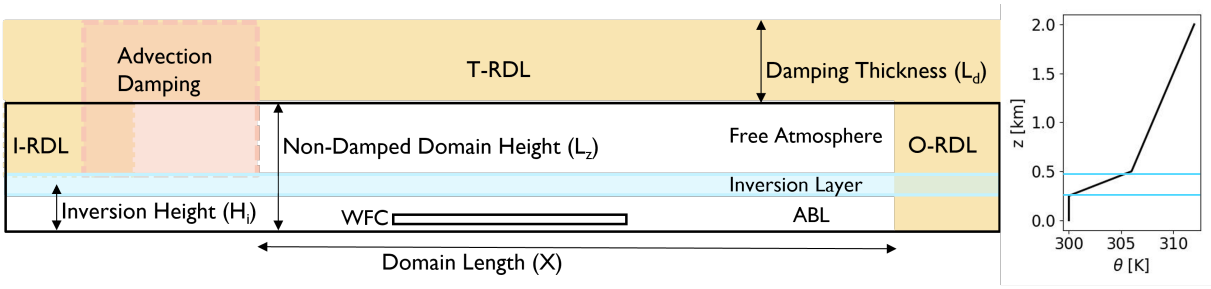


**Figure 1.** (Left) schematic diagram of the numerical setup showing the configuration of advection damping and RDLs at the inlet, top, and outlet (I-RDL, T-RDL, and O-RDL) used to simulate the wind farm canopy, and (right) a CNBL potential temperature profile.

corresponding to $H_i = [150\ m, 500\ m, 750\ m, 1450\ m]$ are initially simulated. The inversion layer thickness in all cases is 100 $m$, and $\Delta\theta = 6\ K$ for the results reported in section 3. Then, the Coriolis force is included in the same setups to investigate its impact on the choice of RDL reference velocities. The boundary conditions for the turbulent cases are the same, except for ground roughness (with a no-slip boundary condition at the bottom of the domain) and turbulent inflow at the inlet. The domain width is also increased to 2 km to allow turbulence build-up due to ground roughness. The non-damped domain length ($X$), unless mentioned, is 18 km for most simulations. The total domain length includes $X$, the advection damping layer length (10.5 to 15 km), and O-RDL thickness. $L_d$ for all RDLs is 5.25 km; $1.5\lambda_{ver}$ as we simulated $Fr = 0.1$. $L_z$ for each simulation was set to capture one IGW vertical wavelength above the inversion layer; $L_z = H_i + \lambda_{ver} + 50\ m$. The mesh resolution was $20\ m \times 20\ m \times 10\ m$ and $10\ m \times 10\ m \times 10\ m$ for the non-turbulent and turbulent runs, respectively.

## 3. Results and Discussion

The AGW properties depend mainly on $Fr$ and $Fr_i$. We establish links between the AGW properties, domain size, and damping layer characteristics to minimize reflections and prevent spurious waves. The results section recalls the proposed setups from the preliminary study in section 3.1. The first section also compares the proposed setups from SOWFA and TOSCA to ensure consistency between the two finite volume codes. This is relevant because we switched from SOWFA to TOSCA for this study. The validity of the proposed setup for CNBL conditions and the requirement for advection damping to constrain the accumulating wave energy at the inlet are discussed in section 3.2. The impact of the Coriolis force on the choice of reference velocities in RDLs is also highlighted. Finally, in section 3.3, the validity of the refined setup with advection damping for inflow turbulence is addressed. The plots shown in the results section are for the wind farm canopy except for those in fig. 2(left), which are the hill cases.

### *3.1. Proposed setup with only internal gravity waves*

The preliminary study simulated a bell-shaped 2D hill and WFCs for idealized linearly stratified conditions with SOWFA. Domain size and damping layer thickness are related to the effective wavelengths, which depend on the $Fr$. The effective horizontal and vertical wavelengths are the representative length scales of the wave spectrum induced for a particular value of $Fr$. All the waves in the spectrum superimpose to form a wave that might differ from the wave corresponding to the dominant length scale, such as the wind farm canopy or hill length. Thus, scaling the domain size with the dominant length scales is inappropriate. The effective wavelengths can be estimated by the distance between the global maxima and minima on a vertical velocity plot along the horizontal and vertical. A plot from the preliminary study for flow over the 2D hill

is shown in fig. 2(left), which shows minimal reflections (characterized by $Cr$) for the $Fr$ cases when the domain length is greater than the effective horizontal wavelength. $Cr$ is the ratio of downwards to upward wave energies, which are the squares of vertical velocities on vertical planes decomposed into downwards and upwards propagating IGWs, respectively. By simulating the same hill, we tested this finding for two CNBL cases, $Fr_i = [0.92, 0.51]$. The CNBL plots are shifted left as $\lambda_{hor}$ values are smaller by almost half of those estimated for the linearly stratified cases. More importantly, the large dip in $Cr$ for domain lengths greater than the $\lambda_{hor}$ is evident.

Similar results are shown in the preliminary study for domain height and the damping layer thickness to be greater than the effective vertical wavelength to minimize the reflections. Moreover, RDLs, at least at the inlet and top, are suggested with inflow/outflow boundary conditions. The damping coefficient $\xi = 1/\tau N$ is related to the buoyancy frequency $N$, as seen in fig. 2(right). The reflections are shown minimum for a range of $Fr$ when $\xi$ is $1 - 10$. Figure 2(right) also compares SOWFA and TOSCA results using the simulation setup for $Fr = 0.1$ and a WFC. The overlapping $Cr$ plots, except for very weak damping coefficients, confirm the consistency of the proposed setups for TOSCA. These cases used $X$ four times $\lambda_{hor}$, and $L_z$ and $L_d$ equal to $\lambda_{ver}$.

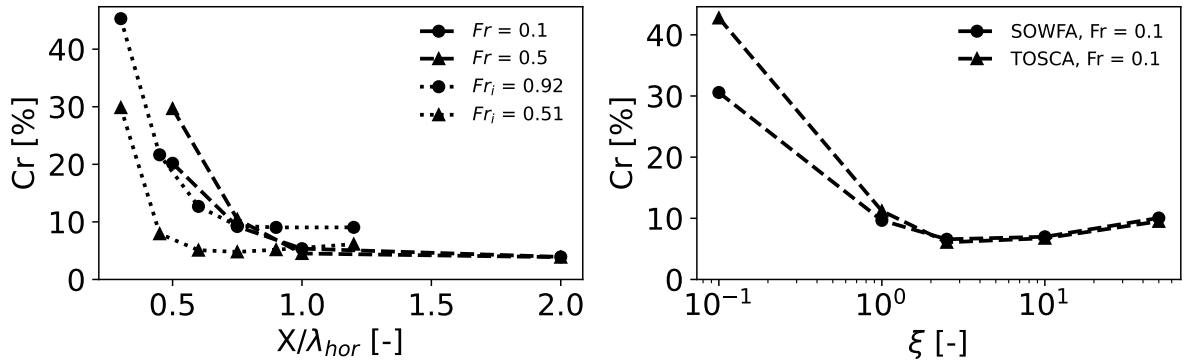


**Figure 2.** Reflection coefficient against (left) $\tilde{X}$ for linearly stratified $[Fr = 0.1, 0.5]$ and CNBL $[Fr_{=}0.92, 0.51]$ hill cases simulated with SOWFA, and (right) $\xi$ for linearly stratified $[Fr = 0.1]$ WFC cases simulated with both SOWFA and TOSCA.

*3.2. The impact of trapped gravity waves on the proposed setup*

Unlike the internal waves, the trapped waves are inside the inversion layer. The TGW properties are mainly dictated by the $Fr_i$, such as increasing wave speed and amplitudes for decreasing $Fr_i$ or vice versa. Based on $Fr_i$, there are three regimes for stationary wave propagation. In the subcritical case ($Fr_i < 1$), the wave speed is greater than the advection speed, and thus, the TGWs can travel up and downstream. In the supercritical case ($Fr_i > 1$), the waves are slower than the advecting flow and can travel only downstream. Meanwhile, in the critical case ($Fr_i = 1$), the TGW speed is the same as the advecting flow. The buoyancy perturbation, proportional to inversion layer displacement, is the highest for critical conditions.

Subcritical conditions can be the most difficult to simulate as the TGWs traveling upstream can enhance the energy accumulation at the inlet. Therefore, we consider four subcritical cases to test and refine the proposed setup suggested in section 3.1. The value of $Fr_i$ was adjusted by varying either $H_i$ or the temperature difference across the inversion layer, which changes $N_i$ for varying potential temperature distribution through the inversion layer. The results in both cases were the same, and only the $H_i$ runs are discussed here. The proposed setup works fine

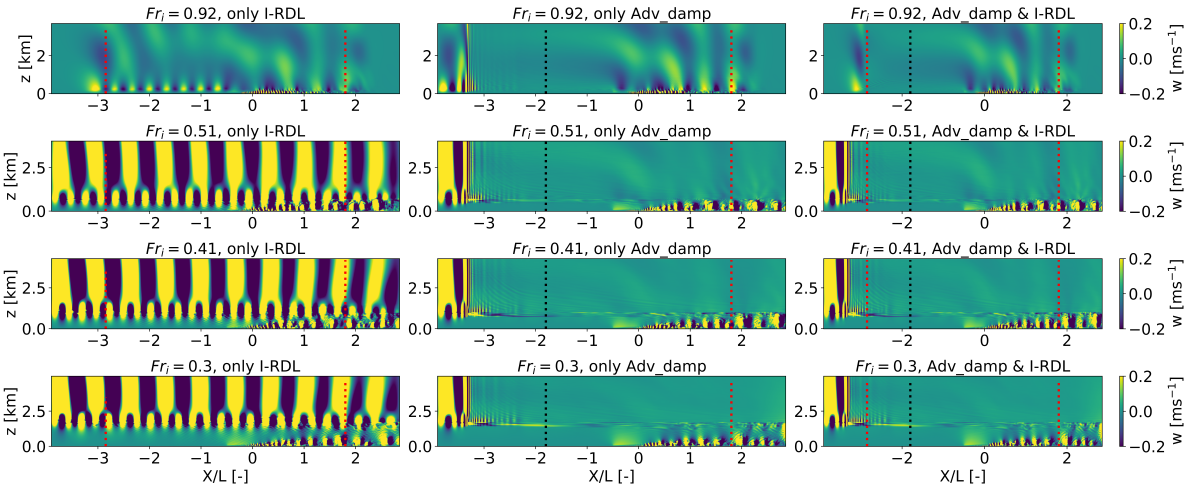


**Figure 3.** Instantaneous vertical velocity at $tN = 200$ through a WFC extending from $-0.5$ to 0.5. (Left): only I-RDL, (middle): only advection damping, and (right): both I-RDL and advection damping at the inlet. The region left of the dotted black line is the advection damping layer, and the regions between the red dotted line and the closest parallel boundary are RDLs.

to handle the WFC-induced IGWs, but the I-RDL cannot retain the accumulating energy as the upstream propagating TGWs bring more energy and much faster than that brought by the IGWs. This can be seen from the instantaneous vertical velocity contours with just the I-RDL in fig. 3(left column). We adopted the advection damping proposed by [3] and tested it for all $Fr_i$ runs. As shown on the vertical velocity plots in fig. 3(middle and right column), the advection damping is effective, with and without the I-RDL, in containing both the accumulated energy at the inlet and the TGWs. Although advection damping alone seems sufficient, runs exceeding a few flow transits through the domain might become contaminated if the I-RDL is not combined with advection damping. We can also see the TGWs amplifying towards the inlet, especially with decreasing $Fr_i$. This is because the TGW wavelength and amplitude increase with increasingly sub-critical conditions. The TGW horizontal wavelengths were estimated to be around 4 to 5 $km$ for $Fr_i = 0.41$ and 0.3, and 1.5 to 3 $km$ for the other two values of $Fr_i$. We observed that advection damping buffer zones matching the TGW horizontal wavelengths work better.

Figure 4(left) shows the reflection coefficient for the simulated $Fr_i$ cases estimated from the temporally averaged vertical velocity fields smoothed towards the damping zones to eliminate the damping layer-induced noise. In most cases in fig. 4(left), $Cr$ is the same with only advection damping and when combined with the I-RDL. More importantly, it is less than 10% for all cases, which, in our experience, is a fairly reflection-free simulation. It is important to note that the $Cr$ metric is very sensitive to wave direction and noise. For instance, the WFC-induced eddies seem to trigger AGWs, seen even on the temporally averaged vertical velocity contour in fig. 4(right). These eddy-induced IGWs propagate randomly as their source is random but still part of the velocity field assessed to calculate $Cr$. This is also the reason for relatively higher $Cr$ values for ($Fr_i = 0.92$) cases, where the inversion layer is close to the WFC and eddy-induced AGWs are prominent. On the other hand, the higher $Cr$ for the least subcritical case $Fr_i = 0.3$ might be the footprint of strong TGWs affecting the flow along the inversion layer in the free atmosphere aloft. Simulating large domains may reduce the reflection, but a proper investigation of the impact of reflections on the blockage effect and wake recovery is essential. Such an investigation is less meaningful with the WFC model; thus, we will address

it with actuator discs/lines modelling of wind farms in a follow-up study.

The effect of the Coriolis force on the choice of reference velocities was also investigated. To this end, we simulated the $Fr_i = 0.41$ case for a few latitudes. We noticed that the Coriolis force has minimal to no impact on the damping setup. The Coriolis force might deflect the flow around the WFC just as it does around a wind farm [6]. However, this deflection may not be felt in the RDLs at least a wavelength away from the WFC.

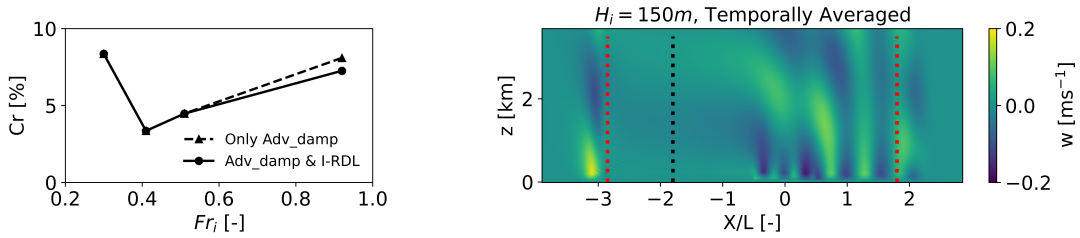


**Figure 4.** (Left) Reflection coefficient computed from temporally averaged vertical velocity fields for the tested $Fr_i$ and (right), vertical velocity for $Fr_i = 0.92$ on a vertical plane temporally averaged over two flow-through times. The averaging period for all cases is 10 s.

*3.3. The impact of turbulence on the proposed setup*

Finally, we investigate the impact of inflow turbulence on the optimized setup. The four $Fr_i$ cases are tested by including Coriolis force for latitude 41.3 $deg$, ground roughness length of 0.01 $m$, and feeding inflow turbulence from precursor simulations. The spin-up time for the precursor simulations was 20 $ks$, and the inflow data were stored for 20 $ks$ beyond spin-up. The eddy size along the streamwise direction is several times $H_i$, and should change for varying boundary layer height [7]. Therefore, the incoming turbulence also induces IGWs, which appear as noise or turbulence in the free atmosphere.

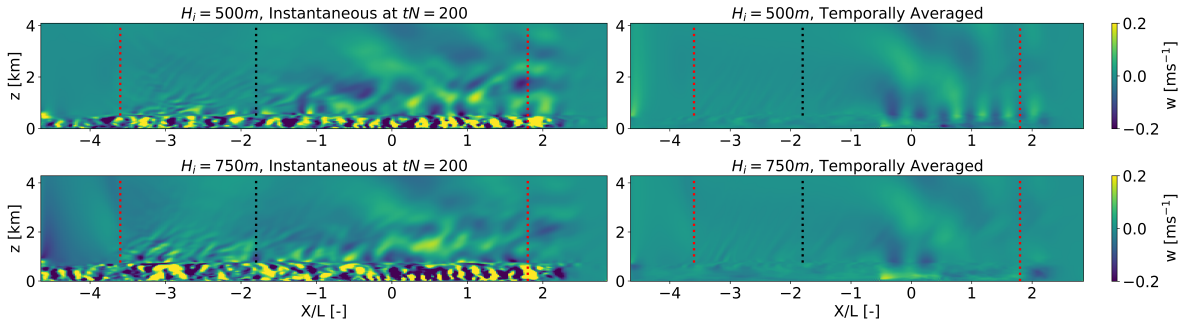


**Figure 5.** (Left) Instantaneous, (right) temporally averaged vertical velocity contours from the turbulent simulations for $Fr$ 0.1, and $Fr_i = 0.51$ and 0.41. The WFC extends from $-0.5$ to 0.5, and the region left of the dotted black line is the advection damping layer. The regions between the red dotted line and the closest parallel boundary are RDLs.

Figure 5(left) shows the instantaneous vertical velocity contours at $tN = 200$ ($N = 0.01$) for $Fr$ 0.1 and $Fr_i$ 0.51, 0.41 in the first and second row, respectively. The relatively high-frequency waves atop the inversion layer are the eddy-induced IGWs, which are not seen in the I-RDL. Moreover, the accumulating energy at the inlet is also contained towards the end of I-RDL,

which overlaps the first advection damping zone. These waves would propagate into the domain parallel to the inlet if advection damping were not there.

The WFC-induced IGWs can be seen on all plots but are more prominent on the temporally averaged vertical velocity contours in fig. 5(right). The averaging period was 5 $s$ over 20 $ks$ of data. The clear AGW signature on the temporally averaged velocity shows that the AGWs are steady as the flow conditions, i.e., $Fr$, $S_h$, $Fr_i$, and $H_i$ were fixed. The WFC-induced IGWs have a greater amplitude for high $Fr_i$ cases, as the inversion layer is closer to the WFC top. The amplitudes, however, diminish to an order of magnitude resembling the eddy-induced IGWs for the low $Fr_i$ cases.Unlike the plots in the left column, only some traces of the eddy-induced IGWs are seen. Thus, it is evident that the most eddy-induced IGWs are averaged out just like their source, turbulence. We show $Fr_i$ 0.51 and 0.41 cases as $H_i$ $500m$ and $750m$ are more practical CNBLs. Simulating $H_i$ $150m$ and $1450m$ is to get initial insight into the AGW dynamics for stable and unstable surface conditions, respectively. We plan to extend this study to stable surface conditions, as the AGWs might be the strongest because of low inversion heights.

$Cr$, estimated from the temporally averaged vertical velocities, is 9.8% and 12% for $Fr_i$ 0.51 and 0.41, respectively. The eddy-induced IGWs, both from the WFC and inflow turbulence, are still visible in the free atmosphere and are indeed captured by $Cr$. The proposed approach in the preliminary study with advection damping is promising for setting up wind farm simulations, including wind farm-induced AGWs. The possibility of eddy-induced IGWs and their interaction with wind farm-induced IGWs requires further investigation, preferably by relating the eddy size to the eddy-induced IGWs.

## 4. Conclusions and Recommendations

This study extends the links between the atmospheric gravity wave properties and critical simulation parameters to simulate wind farm-induced AGWs under CNBL conditions. The Rayleigh damping layers effectively damp IGWs at the top and outlet boundaries, and the advection damping layers seem to constrain the reflections and energy accumulation at the inlet. However, the configuration of these numerical approaches to handle spurious waves in wind farm simulations is ad-hoc. This study gives systematic quantifiable recommendations on implementing RDLs and advection damping layers in simulations with inflow/outflow boundary conditions solved with finite volume LES codes.

We identified the key physical and simulation parameters in simulating wind farm-induced AGWs by dimensional analysis informed of preliminary results. We noticed that the AGW wavelength, amplitude, and direction vary with varying $Fr$ and $Fr_i$. The preliminary study linked the IGW properties to simulation parameters based on simulating 2D hill and WFC for idealized linearly stratified conditions. We test and extend the proposed links to CNBL conditions by simulating WFCs, including Coriolis force, ground roughness, and inflow turbulence.

The proposed setups in the preliminary study are valid for CNBL cases with one main modification. The inlet-RDL cannot contain energy accumulating at the inlet, triggering spurious waves. Thus, advection damping is tested with and without an inlet-RDL to retain the accumulating wave energy at the inlet. We suggest using advection damping at the inlet and RDLs at the inlet and top for runs that persist for a few flow transits through the domain. If computational resources are sufficient, an RDL at the outlet would further reduce the reflections. The buffer zone of the advection damping layer should be greater than the TGW horizontal wavelengths. These wavelengths can be estimated from vertical velocity plots along the domain length at the vertical start of the inversion. We noticed the TGW amplitudes increase for decreasing $Fr_i$, amplifying over simulation time as they are not damped. The Rayleigh damping layers are only a function of one damping coefficient, normally set to dampen the IGWs. An implementation allowing piece-wise damping coefficients in the vertical direction may dampen

the TGWs in the inversion layer if a damping coefficient scaled with the inversion buoyancy frequency is used.

The Coriolis force has little to no impact on the setup as far as reference velocity components matching the geostrophic velocity components are used in the RDLs. The inflow turbulence has larger eddies for smaller $Fr_i$ due to increasing $H_i$, and these eddies seem to displace the inversion layer and induce IGWs of amplitudes similar to the WFC-induced IGWs. However, further investigation is required to establish the eddy-induced IGWs.

The overall systematic approach to simulate wind farm-induced AGWs is to compute $Fr$ and $Fr_i$, and estimate the effective horizontal and vertical wavelengths accordingly. The domain length should be greater than the effective horizontal wavelength, and the non-damped domain height should include the inversion layer and at least one effective vertical wavelength. The RDL thickness should be greater than the effective vertical wavelength, and the buffer zone of the advection damping layer should accommodate at least one TGW horizontal wavelength. The RDL damping coefficient should be 1 to 10 on the scale normalized with $N$. A similar range might work for damping TGWs in the inversion layer, but the damping coefficient should relate to the buoyancy frequency in the inversion layer.

## Acknowledgments

This publication is part of the project: Numerical modelling of Regional-Scale Wind Farm Flow Dynamics, with project number: 2023/ENW/01454045 of the research programme: ENW which is (partly) financed by the Dutch Research Council (NWO). We also acknowledge the active support from Sebastiano Stipa for implementing specific tools of our use in TOSCA.

## References

[1] Allaerts, D. *Ph.D. Thesis: Large-eddy Simulation of Wind Farms in Conventionally Neutral and Stable Atmospheric Boundary Layers* **Tech. rep., 2016**

[2] Smith R.B *Gravity wave effects on wind farm efficiency*, **Wind Energy, 13, 449–458**, https://doi.org/10.1002/WE.366, 2010

[3] Lanzilao, L. and Meyers, J. *An improved fringe-region technique for the representation of gravity waves in large-eddy simulation with application to wind farms*, **http://arxiv.org/abs/2205.10612, 2022.**

[4] Stipa, S., Ajay, A., Allaerts, D., and Brinkerhoff, J. *TOSCA - An Open-Source Finite-Volume LES Environment for Wind Farm Flows* **Wind Energy Science, 2023.**

[5] Chruchefield, M. Sang, L. and Moriarty, P. Overview of the simulator for wind farm application (SOWFA), **National Renewable Energy Laboratory, 2012.**

[6] Gadde, S, N. and Stevencs, R,J,A,M. Effect of Coriolis force on a wind farm wake, **Journal of Physics: Conference Series, 1256, 012-026**, https://dx.doi.org/10.1088/1742-6596/1256/1/012026, 2019

[7] Brooke, J. Stanislawski. Thedin, R. Sharma, A. Branlard, E. Vijayakumar, G. Michael, A. Sprague. Effect of the integral length scales of turbulent inflows on wind turbine loads, **Renewable Energy, 217, 119-218**, https://doi.org/10.1016/j.renene.2023.119218, 2023

[8] Allaerts, D. and Meyers, J. *Annual impact of wind-farm gravity waves on the Belgian-Dutch offshore wind-farm cluster*, **Journal of Physics: Conference Series, 1037, 7, 2018**, doi = 10.1088/1742-6596/1037/7/072006, ISSN = 1742-6596

[9] Lanzilao, L. and Meyers, J., *A parametric large-eddy simulation study of wind-farm blockage and gravity waves in conventionally neutral boundary layers* 2023, archiveprefix = arXiv, eprint = 2306.08633, primaryclass = physics.flu-dyn

[10] Dale, Durran R., *Nonreflecting Boundary Conditions*, **Springer, 395–438, 1999**, doi = 10.1007/978/1/4757/3081/4/8, https://link.springer.com/chapter/10.1007/978/1/4757/3081/4/8

[11] Khan, M, A. Allaerts, D. Watson, S. and Churchfield, M., *Investigating the Relationship between Simulation Parameters and Flow Variables in Simulating Atmospheric Gravity Waves in Wind Energy Applications*, 2024, archiveprefix = arXiv, submissionidentifier = submit/5489415, primaryclass =physics.flu-dyn

[12] Stipa, S. and Ahmed Khan, M. and Allaerts, D. and Brinkerhoff, J., *An LES Model for Wind Farm-Induced Atmospheric Gravity Wave Effects Inside Conventionally Neutral Boundary Layers*, **Wind Energy Science Discussions, 1-22, 2024**, https://wes.copernicus.org/preprints/wes-2023-171/, 10.5194/wes-2023-171